Variations of Vibronic States in Densely Packed Structures of Molecules with Intramolecular Dipoles

*Sergey Trishin, Christian Lotze, Johanna Richter, Gaël Reecht, Nils Krane, Philipp Rietsch, Siegfried Eigler, and Katharina J. Franke**

Electrostatic potentials strongly affect molecular energy levels and charge states, providing the fascinating opportunity of molecular gating. Their influence on molecular vibrations remains less explored. Here, we investigate ethyl-diaminodicyanoquinone molecules on a monolayer of MoS_2 on Au(111) using scanning tunneling and atomic force microscopy and spectroscopy. These molecules exhibit a large dipole moment in gas phase, which is found to (partially) persist on the MoS_2 monolayer. The self-assembled structures consist of chains, where the dipoles of neighboring molecules are aligned antiparallel. Thanks to the decoupling efficiency of the molecular states from the metal by the MoS_2 interlayer, vibronic states of the molecules are resolved, which vary in intensity depending on the molecular surrounding. We suggest that the vibrations are strongly damped by electrostatic interactions with the environment.

1. Introduction

Molecules adsorbed on surfaces constitute a versatile platform for the design of hybrid organic–inorganic devices.[1,2] The energy-level alignment is largely determined by the interactions between the molecule and the substrate due to hybridization, charge transfer, and screening.[3–5] These effects are particularly strong when the molecules are in direct contact to a metal substrate, often leading to the loss of molecular function and tunability. To maintain the molecular properties, inorganic insulating or semiconducting interlayers have been inserted between the molecules and metal substrate.[6–11] The decoupling is also

S. Trishin, C. Lotze, J. Richter, G. Reecht, N. Krane, K. J. Franke
Fachbereich Physik
Freie Universität Berlin
14195 Berlin, Germany
E-mail: franke@physik.fu-berlin.de

P. Rietsch, S. Eigler
Institut für Chemie und Biochemie
Freie Universität Berlin
14195 Berlin, Germany

beneficial for spectroscopic investigations of the molecular states, as the excitations are long-lived. The corresponding narrow linewidths then allow for the resolution of densely spaced spectroscopic features, such as vibronic states.[6,9,10,12–16]

Although the interlayers decouple the molecules from the substrate, there may still be charge transfer depending on the alignment of the energy levels of the molecules with respect to the Fermi level of the underlying metal.[1,17] Control of the charge state is highly desirable for devices and may be achieved by a gate electrode.[18,19] However, the implementation of a gate electrode is not always feasible in experiment. Other strategies rely on the control of the charge state by self-assembly of donor and acceptor molecules,[20] ideally on the decoupling layers.[21] Recently, it has been shown that the presence of a molecular dipole can be used for tuning the energy-level alignment of neighboring molecules and, thus, gain control over the charge state.[22,23] This approach also offers the unique opportunity to investigate the effect of local electrostatic potentials on the molecular properties. One interesting aspect is the modification of molecular vibrations in the presence of an electric field. It has been found that approaching a scanning tunneling microscopy (STM) tip to a molecule leads to a shift of the vibrational modes.[24–26] However, in this case, it is difficult to disentangle the influence of chemical forces from the electrostatic forces.

Here, we aim at resolving the effect of electrostatic forces on molecular vibrations by control of the molecular environment. For this, we chose a molecule with a large intrinsic dipole moment to create a structure with non-negligible electrostatic potential. Ethyl-diaminodicyanoquinone (ethyl-DADQ) consists of two charge-separated moieties—an electronegative dicyanomethylene group and an electropositive imidazolidine group (**Figure 1**d)—which result in a large dipole moment of around 17.3 Debye in gas phase.[27] Surprisingly, this dipole moment was found to be enlarged when the molecule is in contact to a metal substrate due to charge transfer.[28] The interaction with the substrate prohibited the resolution of vibronic states. Hence, we now use a monolayer of MoS_2 for decoupling the molecules from the metal substrate. We find that the molecules self-assemble in quasi-1D arrangements and preserve a dipole moment. The decoupling efficiency allows us to detect vibronic states, which we find to be strongly suppressed in densely packed molecular chains. We speculate that intermolecular
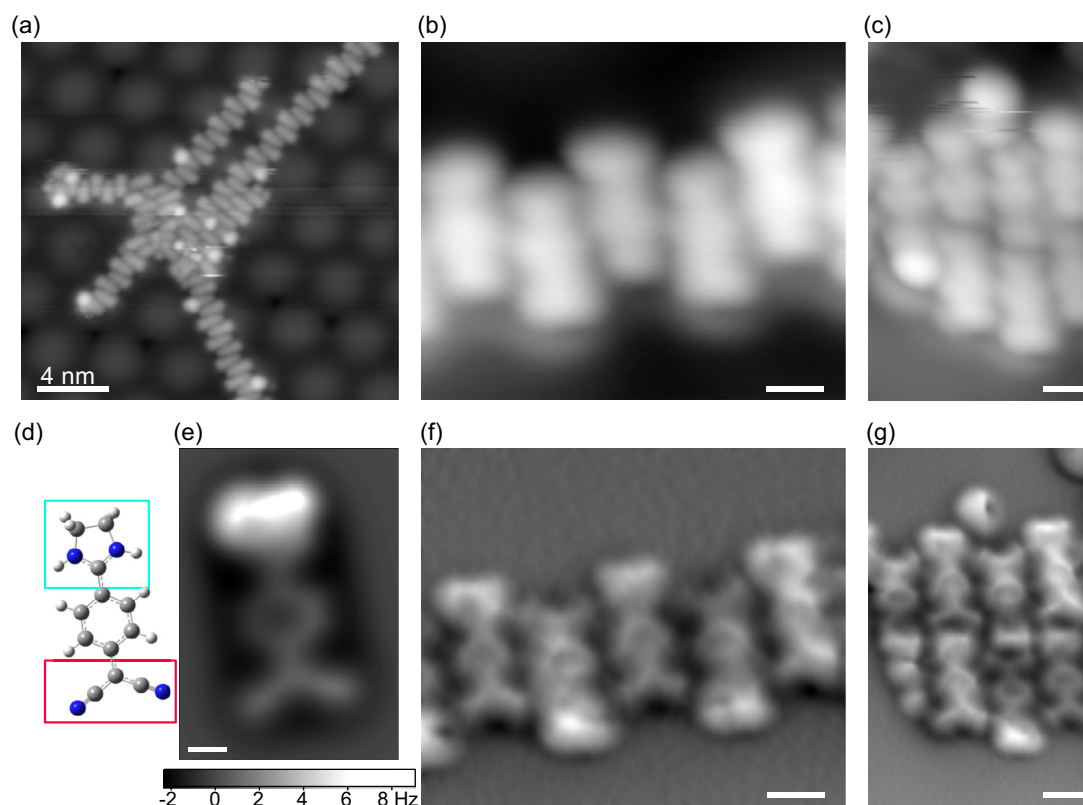
Figure 1. a) STM topography of ethyl-DADQ adsorbed on a monolayer of MoS$_2$/Au(111). b) STM image taken with a Cl-functionalized tip of a single-stranded molecular chain. c) STM image taken with a Cl-functionalized tip of a double-stranded molecular chain. d) Stick-and-ball model of the ethyl-DADQ molecule. It consists of a benzene ring, which has two moieties bound to it: an imidazolidine group (top, teal) and a dicyanomethylene group (bottom, red). e) The molecule has been placed on a graphene sheet for mimicking the van der Waals interactions with the surface. Based on this structure, we simulated the frequency-shift signal of the ethyl-DADQ when probed at constant-height with tip-sample distance of 6.9 Å employing the probe particle model.[31,46] The legend below the map gives the Δf signal in units of Hz. The map is to scale with (d). f,g) Δf images recorded on the same area as the STM images in (b,c). The STM topographies in (a,c) were recorded at a setpoint of 1 V, 30 pA, the one in (b) at 520 mV, 30 pA. The constant-height images in (f,g) were recorded at 1 V, 30 pA. After switching the feedback off, the bias voltage was set to 0 V and the tip approached by 0.1 Å to the substrate. The scale bars in (b,c,f,g) are 5 Å and the one in (e) is 2 Å.

electrostatic interactions lead to a significant damping of the vibrations.

2. Results and Discussion

2.1. Self-Assembly of Ethyl-DADQ Molecules on MoS$_2$

Deposition of ethyl-DADQ molecules at 230 K on a monolayer of MoS$_2$ on an Au(111) substrate leads to the self-assembly in quasi-1D arrangements (Figure 1a). We refer to these molecular structures as chains in the following. The chains follow a preferred orientation with respect to the underlying moiré structure, which forms as a result of a lattice mismatch between the terminating Au layer and the MoS$_2$ and is seen as a hexagonal superstructure with a periodicity of 3.3 nm in the background.[29,30] At low molecular coverage, we find that most chains only consist of a single molecular row, while double stranded chains or even wider chains remain scarce. We discuss the single- and double-stranded chains in the following.

We first analyze the structure of the self-assembled single-stranded chains. These chains consist of a zig-zag arrangement of the molecules, with the individual molecules imaged as an almost oval shape with one termination being slightly thinner than the other one. A similar arrangement has been reported for the same molecules in direct contact to an Au(111) surface.[28] A Cl-functionalized tip (see Methods) enhances the asymmetric appearance of the individual molecules (Figure 1b) and evidences the alternating antiparallel orientation with respect to the nearest neighbors. While the STM image is not conclusive on the orientation of the individual molecules, frequency-shift (Δf) images of the same area allow for an unambiguous identification of the molecular arrangement (Figure 1f). The observed shape directly reflects the atomic structure of the molecule (cp. Figure 1d) with the dicyanomethylene, benzene ring, and imidazolidine group lying flat on the surface. The largest elevation is found at the position of the H atoms at the imidazolidine termination. The experimental images are well reproduced by simulations based on the probe-particle model by Hapala et al.,[31] when the molecules are placed parallel to the surface and the H atoms at the imidazoline

2300105 (2 of 7)

unit point toward the tip (Figure 1e). This detailed insight into the structure reveals that the cyano groups face the imidazolidine group, supporting CN–HN hydrogen bonds, which contribute to the stabilization of the structure.

Using the same Cl-functionalized tip, we also investigated the double-stranded chains. The STM and atomic force microscopy (AFM) images (Figure 1c,g) reveal a similar zig-zag pattern of alternating molecular arrangements along the chains, while the molecules arrange head-to-tail across the chains.

2.2. Intramolecular Dipole

The alternating structure and head-to-tail arrangement of the molecules suggests that electrostatic interactions may also contribute to stabilizing the arrangements assuming that the molecular dipole moment is conserved on the surface. To find out if an intramolecular dipole persists, we mapped the local contact potential difference (LCPD) across the molecules, which is obtained from the maxima of the voltage-dependent frequency-shift $(\Delta f - V)$ curves.[32,33] **Figure 2**a shows the extracted LCPD values from a line of densely spaced spectra along a single ethyl-DADQ located at the end of a single-stranded chain (see Figure 2b). The lowest LCPD value is found above the imidazolidine group. In contrast, the LCPD value increases over the molecule toward the dicyanomethylene group, where it peaks. This distribution is up to our expectations, as the imidazolidine is the positively charged moiety of the molecule, whereas the dicyanomethylene group is negatively charged. The experiments thus let us conclude on the presence of an intramolecular dipole of the ethyl-DADQ on the MoS_2 layer. Unfortunately, we cannot assess the magnitude of the dipole moment from the

experiment. We note that the same molecules in direct contact to Au(111) also revealed the presence of an intramolecular dipole, which was shown to be enhanced as compared to the gas-phase molecule by charge transfer from the substrate.[28]

2.3. Molecular Energy Levels and Vibronic States in Single-Stranded Chains

Next, we turn to the investigation of the electronic structure of the ethyl-DADQ on MoS_2/Au(111). The monolayer of MoS_2 itself exhibits a bandgap around the Fermi level, where the onset of the conduction band is found at ≈ 0.5 V and the valence band maximum is located at ≈ -1.4 V (black spectrum in **Figure 3**a).[29,34] The valence and conduction band edges are smeared out due to hybridization of the S layer with the Au substrate state.[35,36]

Spectra recorded on the ethyl-DADQ molecules (Figure 3a blue and green) show additional peaks at negative bias voltages
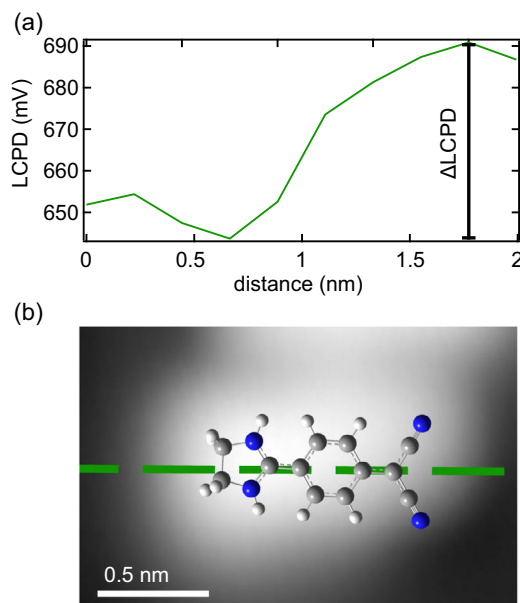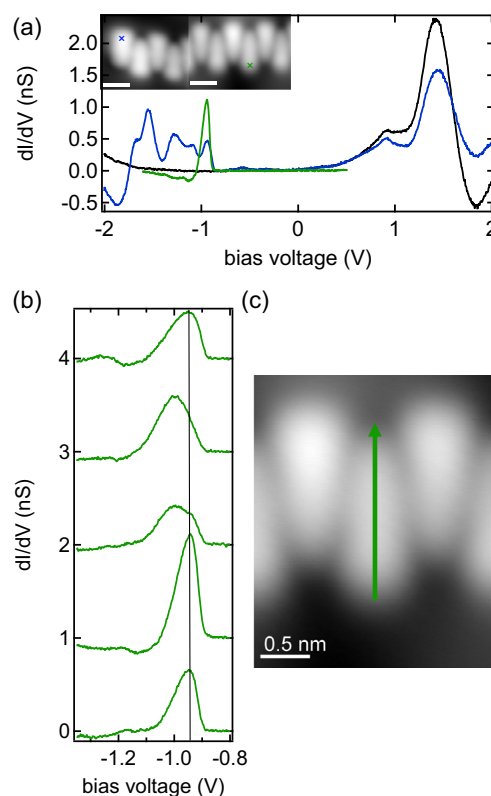

Figure 2. a) Extracted LCPD signal over a line of densely spaced spectra, as indicated with the green dashed line. The spectra were taken at a set-point of −1.6 V, 400 pA. b) STM topography of a molecule at the edge of a one-molecule wide chain. A stick-and-ball structure model was overlaid for clarity. The topography was recorded at a setpoint of 1 V, 30 pA.

Figure 3. a) dI/dV spectra recorded on the monolayer island of MoS_2 on Au(111) shown in black. dI/dV spectra performed on the imidazolidine group of a single ethyl-DADQ at the end of a molecular chain (blue) and a molecule inside a chain (green) with the locations shown in the inset. Several resonances appear inside the electronic bandgap of the MoS_2, which we attribute to tunneling into the HOMO of the molecule and vibronic levels associated with it. The spectra were recorded at setpoints of 2 V, 1 nA (black), −1.6 V, 400 pA (blue), and −1.6 V, 50 pA (green). The scale bars are 1 nm. b) dI/dV spectra performed along the green line indicated in (c). The resonances vary along the molecule as described in the text. The spectra were recorded at a setpoint of −1.6 V, 50 pA and offset by 1 nS for clarity. c) STM topography of a molecular chain. All topographies were recorded at a setpoint of 1 V, 30 pA.

inside the semiconducting gap, corresponding to excitations of a positive ion resonance. The resonance structure (onset at ≈ -0.9 V) is much sharper than observed for the same molecules in direct contact to the Au(111) substrate.[28] The smaller linewidth indicates longer excited state lifetimes and less hybridization with the substrate. These observations are in agreement with earlier studies of organic molecules on MoS_2/Au(111), which pointed out the decoupling efficiency of the monolayer MoS_2.[10,37,38]

The onset of the resonance is followed by a set of additional peaks, which are very pronounced on the molecule at a chains' end (blue spectrum in Figure 3a) and less obvious on molecules embedded inside the bulk of a chain (green spectrum in Figure 3a,b). Sidebands to the ion resonances are typically associated to vibronic states.[6,9,12–16] The strongest peaks originate from the excitation of vibrations with large Huang–Rhys factors, which represent the electron–phonon coupling strength. The strong suppression of the vibronic satellite peaks on molecules surrounded by neighbors suggests a significant damping of the vibrational states.[39,40] We speculate that the dipolar environment strongly affects molecular vibrations, in particular those with dipolar character.

We also observe a local variation of the vibronic spectra along the individual molecules (Figure 3b,c). The spectra on the imidazolidine group show a sharp onset of a peak at −950 mV, with a broader high-energy shoulder. The asymmetric lineshape suggests the presence of at least one vibronic satellite peak. At the center of the molecule, the intensity ratio between shoulder and peak is reversed, corroborating the interpretation of a second peak in the first spectra. The intensity ratio changes again at the dicyanomethylene termination. To map out these changes in intensity ratio, we show constant-height dI/dV maps at the peak energies in **Figure 4**d–g. While the off-resonance map at −900 mV shows the largest intensity on the imidazolidine units, the first map on the molecular resonance at −950 mV shows additional intensity next to the dicyanomethylene group, which gains strength at −1000 mV. The map at −1050 mV remains with the largest intensity between the molecules. To understand these intensity variations, we compare the maps to the theoretical electronic structure of the ethyl-DADQ molecule.

Excitation of a positive ion resonance in tunneling spectroscopy implies probing the occupied molecular orbitals. We calculated the highest occupied molecular orbital (HOMO) of the ethyl-DADQ molecule using density functional theory (see Methods, Figure 4b). When the flat molecule is probed with an s-wave tip at a certain height, the Tersoff–Hamann model[41] predicts the HOMO to appear with a U shape centered on the benzene ring and opening around the dicyanomethylene group (Figure 4c). The small asymmetry in the simulations stems from a torsion of the molecule.

For comparison to the experimental maps, we first need to eliminate the influence of the topographic height of the ethyl-DADQ on the surface. The off-resonance map at −900 mV (Figure 4d) revealed intensity at the imidazolidine group, indicating an elevated height in agreement with the AFM images in Figure 1. Neglecting the intensity at the imidazolidine group, the remaining intensity around the dicyanomethylene group on the resonance (at −950 mV) resembles the Tersoff–Hamann map. We thus ascribe the first resonance within the MoS_2 gap to tunneling through the HOMO. The very different
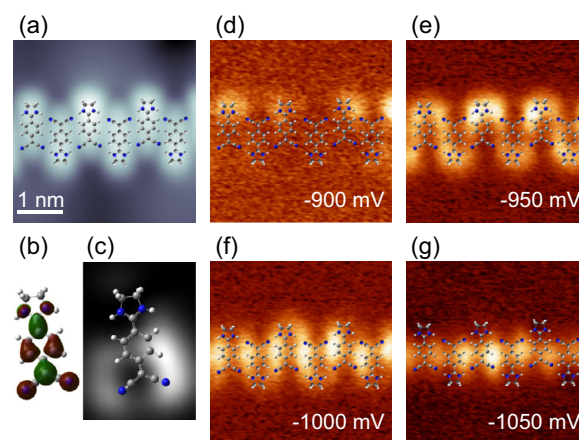

Figure 4. a) STM topography of a single-stranded chain of ethyl-DADQ molecules. b) DFT simulation of the HOMO of the ethyl-DADQ placed on a sheet of graphene (see Methods for details). c) Simulated Tersoff–Hamann constant-height image of the HOMO using an s-wave tip at a distance of 5 Å above the molecule. The most pronounced shape is U-like around the dicyanomethylene group. The asymmetry in the images originates in a torsion of the molecule. Due to steric hindrance, the imidazolidine group is rotated with respect to the phenyl group. d–g) Constant-height dI/dV maps taken at the same location as the topography in (a). The energies of the maps are indicated in the bottom-right corner. All images were taken at an initial setpoint of 1 V, 30 pA before the feedback was switched off; the tip was additionally approached toward the sample by 2 Å.

intensity distribution at higher energies does not agree with the shape of the HOMO. A simple vibronic excitation associated to the HOMO, thus, cannot account for this map. As the HOMO-1 is found separated by 1.3 eV from the HOMO in gas-phase calculations, the different shape can also not be explained by excitation of a low-lying orbital. Instead, we suggest that vibration-assisted tunneling contributes to the unexpected distribution of the differential conductance signal. In a simple picture, an increased intensity at the nodal planes of a molecular orbital can arise from the inelastic excitation of an out-of-plane mode, which changes the wavefunction overlap with the tip. In case of an asymmetric mode around a nodal plane, an increase in the tunneling matrix element leads to a new vibration-assisted tunneling channel[37,42] and thus to increased conductance at positions where the undressed molecular orbitals do not contribute much to the tunneling signal. This model—together with the topographic influence—could account for the variation of peak heights in Figure 3b and the deviation from plain orbital shapes in Figure 4e–g.

We now recall that the spectra varied significantly between molecules embedded in the chain and at the chain's termination (Figure 3a). This indicates that the molecular environment affects the molecular vibrations and, thus, also the vibration-assisted tunneling.

2.4. Vibronic and Vibration-Assisted Tunneling Spectra in Double-Stranded Molecular Chains

To unravel the influence of the electronic environment, we investigated the vibronic and vibration-assisted sidebands to
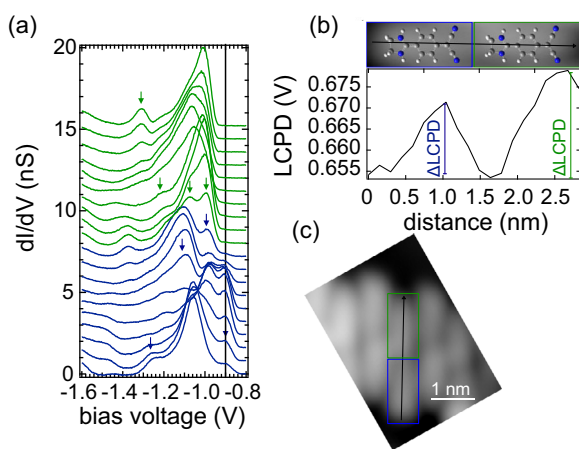
Figure 5. a) dI/dV spectra around the first positive ion resonance performed along molecules of a double-stranded chain, as indicated in (c). The spectra are offset for clarity. The arrows indicate the position of the most pronounced resonances. Blue and green spectra correspond to the blue and green boxed molecule in (c). The spectra are offset by 0.8 nS for clarity. b) LCPD values extracted from measurements at the same positions as those in (a) and shown above the graph. c) STM topography of a double-stranded chain. The colored boxes indicate the two probed molecules in (a,b), which have a different electrostatic environment. STM images were recorded with a setpoint of 1 V, 30 pA; the spectra were recorded at a setpoint of −1.6 V, 100 pA with the tip being additionally approached toward the sample by 0.6 Å.
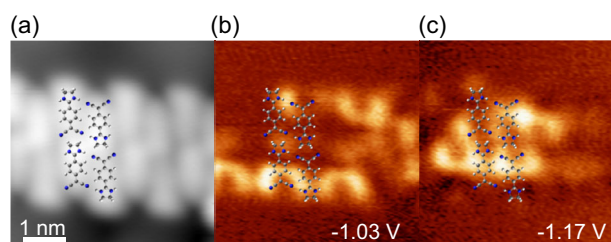

Figure 6. a) STM topography of a double-stranded chain of ethyl-DADQ molecules. A molecular model is superimposed on the image for better comparison. b,c) Constant-height dI/dV maps taken at the same location as the topography in (a). The energies of the maps are indicated in the bottom-right corner. All images were taken at an initial setpoint of 1 V, 30 pA; the tip was additionally approached toward the sample by 2 Å.

the HOMO-derived resonance of the ethyl-DADQ molecules in the double-stranded chains (**Figure 5**). As shown above, the molecular orientation along these chains is similar to the one in the single-stranded chains with a second row added in parallel. This assembly imposes different electronic environments to the molecules within the chain. Half of the molecules have the imidazolidine group sticking out of the chain (indicated with the blue box in 5c) and the other half of the molecules are embedded more inside the chain (indicated with the green box).

To resolve how this structure affects the electronic properties of the molecules, we recorded a line of densely spaced spectra along a molecular row, as indicated with the black arrow in Figure 5c. The results are shown in Figure 5a with the color code identifying the corresponding boxed molecules in the topography.

Describing first the blue spectra, one can see that several peaks emerge, which are marked with the blue arrows. Mainly four different resonances can be resolved, at energies of around −900, −980, −1100, and −1270 mV, with their intensities varying along the molecule. Whereas the resonance at −900 mV has a very low intensity at the imidazolidine group of the molecule and is strongest in the center, the resonances at −1100 and −1270 mV have their main contribution to the signal at the terminations of the molecule. The resonance at −980 mV is mainly located at the center and the dicyanomethylene group of the molecule. The spectra taken along the green boxed molecule are not a simple repetition of the spectra. First, we note that the onset of the resonance structure is shifted by ≈90 mV to higher energies. We then resolve again four resonances with varying intensity along the molecules (at −990, −1075, −1220, and

−1300 mV). The overall shift can be explained by different screening from the environment due to different location of the molecule on the moiré structure and the different molecular neighborhood.[5] However, the resonance sidebands are not simply subject to a rigid shift. The intensity variations again point to a significant damping of the molecular vibrations due to the different electrostatic environment, which is different for the two ethyl-DADQ molecules.

To probe the electrostatic environment, we present the LCPD along the same two molecules in Figure 5b. The spatial variation along both molecules is in agreement with the presence of an intramolecular dipole albeit with a different strength of the two molecules. The molecular environment is thus also expressed in different screening of the molecular dipole. The variations in vibronic damping may thus be correlated with the electrostatic potential imposed by the environment.

In the last step, we again map out the molecular resonance structure for comparison with the vibronic spectra (**Figure 6**). The map at −1030 mV shows some ethyl-DADQ molecules with the shape of the HOMO as expected from the Tersoff–Hamann simulations in Figure 4c. In contrast to the single-stranded chains, these maps are thus not strongly influenced by an elevated imidazolidine group and, therefore suggest a flatter adsorption configuration. The different onsets of the molecular resonances observed in Figure 5a are reflected by some molecules still being dark at this bias voltage. At this particular bias voltage, the molecules with high intensity are those equivalent to the ethyl-DADQ molecules indicated in green. The maps thus clearly reflect the alternating electronic structure of the molecules sticking out of the chains compared to the ones embedded deeper in the chain. At larger bias voltage, the dI/dV signal gains strength again between the molecules, similar to the earlier observation on the single-stranded chains. This again shows that vibration-assisted tunneling dominates the vibronic spectra.

3. Conclusions

We investigated organic molecules (ethyl-DADQ) on a monolayer of MoS_2 on Au(111) using scanning tunneling and atomic force microscopy and spectroscopy. These molecules were chosen for their large intramolecular dipole moment which raises the question of electrostatic intermolecular interactions and their

effect on the properties of the layer. Importantly, we first showed that an intramolecular dipole moment is preserved within the self-assembled molecular arrangements. The MoS_2 decoupling layer then allowed us to resolve vibronic states of the individual molecules. Our main observation is a strong variation of the vibronic structure depending on the molecular surrounding. We ascribe the strong suppression of vibronic and vibration-assisted tunneling to damping of the vibrational modes. We speculate that the damping mainly originates in the anisotropic electrostatic potential imposed by the electrostatic dipoles of the neighboring ethyl-DADQ molecules. Our results suggest that the electrostatic environment can be used to tune the strength of damping and stiffening of molecular vibrations. Indeed, damping may be beneficial for the performance of molecular-scale devices.

4. Experimental Section

The Au(111) substrate was cleaned by repeated sputter-annealing cycles in an ultrahigh vacuum chamber. The MoS_2 islands were subsequently grown by depositing Mo atoms in H_2S gas of $p = 2 \times 10^{-5}$ mbar and simultaneous annealing of the gold substrate to 800 K. The ethyl-DADQ molecules were deposited at a substrate temperature of 230 K. The as-prepared sample was transferred into the scanning tunneling microscope. The microscope is equipped with a qPlus sensor allowing for simultaneous measurements of the tunneling current and frequency shift.[43] The base temperature was 4.5 K.

The LCPD value was determined from bias-dependent frequency-shift spectra ($\Delta f - V$). The frequency shift depends quadratically on the applied bias voltage. The maximum of the inverse parabola corresponds to the LCPD. Its value is extracted from a fit.

To image molecules at very short tip-molecule distances, an in situ functionalization of the tip is required. We attached chlorine atoms to the tip by picking them up from chlorinated Fe-octaethyl-porphyrin molecules codeposited on the same substrate. Such a tip has been used for taking the STM and simultaneous AFM images in Figure 1b,c,f,g. Otherwise we used an Au-coated tip for STM measurements and dI/dV spectroscopy.

DFT calculations of the ethyl-DADQ molecules were performed employing the Gaussian 16 A.03 package, using the 6–31++G(d,p) basis set and the B3PW91 functional.[44] For structure optimization, the molecule was placed on a graphene sheet applying the ONIOM method and using the UFF force field for the graphene atoms, to mimic the weak interaction with the surface.[45] As a result, the molecular structure is flattened as compared to a gas-phase optimized single molecule (dihedral angle of $\approx4°$ vs $\approx7°$ between the benzene and imidazolidine group. This flattened structure shows similar orbital shapes and simulated STM Tersoff–Hamann images to the nonflat molecule but shows significantly better agreement of the simulated AFM Δf images with the experimental ones.

Conflict of Interest

The authors declare no conflict of interest.

Data Availability Statement

The data that support the findings of this study are available from the corresponding author upon reasonable request.

[1] D. Xiang, X. Wang, C. Jia, T. Lee, X. Guo, Chem. Rev. 2016, 116, 4318.

[2] D. P. Goronzy, M. Ebrahimi, F. Rosei, . Arramel, Y. Fang, S. De Feyter, S. L. Tait, C. Wang, P. H. Beton, A. T. S. Wee, P. S. Weiss, D. F. Perepichka, ACS Nano 2018, 12, 7445, pMID: 30010321.

[3] S. Braun, W. R. Salaneck, M. Fahlman, Adv. Mater. 2009, 21, 1450.

[4] R. Otero, A. L. Vazquez de Parga, J. M. Gallego, Surf. Sci. Rep. 2017, 72, 105.

[5] I. F. Torrente, K. J. Franke, J. I. Pascual, J. Phys.: Condens. Matter 2008, 20, 184001.

[6] X. H. Qiu, G. V. Nazin, W. Ho, Phys. Rev. Lett. 2004, 92, 206102.

[7] J. Repp, G. Meyer, S. M. Stojković, A. Gourdon, C. Joachim, Phys. Rev. Lett. 2005, 94, 026803.

[8] M. Garnica, D. Stradi, S. Barja, F. Calleja, C. Díaz, M. Alcamí, N. Martín, A. L. Vázquez de Parga, F. Martín, R. Miranda, Nat. Phys. 2013, 9, 368.

[9] F. Schulz, R. Drost, S. Hämäläinen, P. Liljeroth, ACS Nano 2013, 7, 11121.

[10] N. Krane, C. Lotze, G. Reecht, L. Zhang, A. L. Briseno, K. J. Franke, ACS Nano 2018, 12, 11698.

[11] X. Yang, I. Krieger, D. Lüftner, S. Weiß, T. Heepenstrick, M. Hollerer, P. Hurdax, G. Koller, M. Sokolowski, P. Puschnig, M. G. Ramsey, F. S. Tautz, S. Soubatch, Chem. Commun. 2018, 54, 9039.

[12] N. A. Pradhan, N. Liu, W. Ho, J. Phys. Chem. B 2005, 109, 8513.

[13] N. Ogawa, G. Mikaelian, W. Ho, Phys. Rev. Lett. 2007, 98, 166103.

[14] F. Matino, G. Schull, F. Köhler, S. Gabutti, M. Mayor, R. Berndt, Proc. Natl. Acad. Sci. 2011, 108, 961.

[15] K. J. Franke, J. I. Pascual, J. Phys.: Condens. Matter 2012, 24, 394002.

[16] A. Mehler, N. Néel, M.-L. Bocquet, J. Kröger, J. Phys.: Condens. Matter 2018, 31, 065001.

[17] M. Willenbockel, D. Lüftner, B. Stadtmüller, G. Koller, C. Kumpf, S. Soubatch, P. Puschnig, M. G. Ramsey, F. S. Tautz, Phys. Chem. Chem. Phys. 2015, 17, 1530.

[18] A. Riss, S. Wickenburg, L. Z. Tan, H.-Z. Tsai, Y. Kim, J. Lu, A. J. Bradley, M. M. Ugeda, K. L. Meaker, K. Watanabe, T. Taniguchi, A. Zettl, F. R. Fischer, S. G. Louie, M. F. Crommie, ACS Nano 2014, 8, 5395.

[19] S. Wickenburg, J. Lu, J. Lischner, H.-Z. Tsai, A. A. Omrani, A. Riss, C. Karrasch, A. Bradley, H. S. Jung, R. Khajeh, D. Wong, K. Watanabe, T. Taniguchi, A. Zettl, A. H. C. Neto, S. G. Louie, M. F. Crommie, Nat. Commun. 2016, 7, 13553.

[20] I. Fernández-Torrente, K. J. Franke, J. I. Pascual, Phys. Rev. Lett. 2008, 101, 217203.

[21] A. Kumar, K. Banerjee, M. M. Ervasti, S. Kezilebieke, M. Dvorak, P. Rinke, A. Harju, P. Liljeroth, ACS Nano 2021, 15, 9945.

[22] J. Homberg, A. Weismann, R. Berndt, M. Gruber, ACS Nano 2020, 14, 17387.

[23] C. Li, J. Homberg, A. Weismann, R. Berndt, *ACS Nano* **2022**, *16*, 16987.

[24] L. Vitali, R. Ohmann, K. Kern, A. Garcia-Lekue, T. Frederiksen, D. Sanchez-Portal, A. Arnau, *Nano Lett.* **2010**, *10*, 657.

[25] N. Okabayashi, A. Peronio, M. Paulsson, T. Arai, F. J. Giessibl, *Proc. Natl. Acad. Sci.* **2018**, *115*, 4571.

[26] J. Homberg, A. Weismann, T. Markussen, R. Berndt, *Phys. Rev. Lett.* **2022**, *129*, 116801.

[27] P. Rietsch, F. Witte, S. Sobottka, G. Germer, A. Becker, A. Güttler, B. Sarkar, B. Paulus, U. Resch-Genger, S. Eigler, *Angew. Chem. Int. Ed.* **2019**, *58*, 8235.

[28] S. Trishin, T. Müller, D. Rolf, C. Lotze, P. Rietsch, S. Eigler, B. Meyer, K. J. Franke, *J. Phys. Chem. C* **2022**, *126*, 7667.

[29] N. Krane, C. Lotze, K. J. Franke, *Surf. Sci.* **2018**, *678*, 136.

[30] H. Bana, E. Travaglia, L. Bignardi, P. Lacovig, C. E. Sanders, M. Dendzik, M. Michiardi, M. Bianchi, D. Lizzit, F. Presel, D. D. Angelis, N. Apostol, P. K. Das, J. Fujii, I. Vobornik, R. Larciprete, A. Baraldi, P. Hofmann, S. Lizzit, *2D Mater.* **2018**, *5*, 035012.

[31] P. Hapala, G. Kichin, C. Wagner, F. S. Tautz, R. Temirov, P. Jelínek, *Phys. Rev. B* **2014**, *90*, 085421.

[32] L. Gross, F. Mohn, P. Liljeroth, J. Repp, F. J. Giessibl, G. Meyer, *Science* **2009**, *324*, 1428.

[33] F. Mohn, L. Gross, N. Moll, G. Meyer, *Nat. Nanotechnol.* **2012**, *7*, 227.

[34] J. Miwa, S. Ulstrup, S. G. Sørensen, M. Dendzik, A. Grubisić Cabo, M. Bianchi, J. V. Lauritsen, P. Hofmann, *Phys. Rev. Lett.* **2014**, *114*, 046802.

[35] A. Bruix, J. A. Miwa, N. Hauptmann, D. Wegner, S. Ulstrup, S. S. Grønborg, C. E. Sanders, M. Dendzik, A. Grubišić Čabo, M. Bianchi, J. V. Lauritsen, A. A. Khajetoorians, B. Hammer, P. Hofmann, *Phys. Rev. B* **2016**, *93*, 165422.

[36] N. Krane, C. Lotze, J. M. Läger, G. Reecht, K. J. Franke, *Nano Lett.* **2016**, *16*, 5163.

[37] G. Reecht, N. Krane, C. Lotze, L. Zhang, A. L. Briseno, K. J. Franke, *Phys. Rev. Lett.* **2020**, *124*, 116804.

[38] A. Yousofnejad, G. Reecht, N. Krane, C. Lotze, K. J. Franke, *Beilstein J. Nanotechnol.* **2020**, *11*, 1062.

[39] J. Repp, G. Meyer, S. Paavilainen, F. E. Olsson, M. Persson, *Phys. Rev. Lett.* **2005**, *95*, 225503.

[40] S. Fatayer, B. Schuler, W. Steurer, I. Scivetti, J. Repp, L. Gross, M. Persson, G. Meyer, *Nat. Nanotechnol.* **2018**, *13*, 376.

[41] J. Tersoff, D. R. Hamann, *Phys. Rev. B* **1985**, *31*, 805.

[42] N. Pavlicek, I. Swart, J. Niedenführ, G. Meyer, J. Repp, *Phys. Rev. Lett.* **2013**, *110*, 136101.

[43] F. J. Giessibl, *Appl. Phys. Lett.* **2000**, *76*, 1470.

[44] M. J. Frisch, G. W. Trucks, H. B. Schlegel, G. E. Scuseria, M. A. Robb, J. R. Cheeseman, G. Scalmani, V. Barone, B. Mennucci, G. A. Petersson, H. Nakatsuji, M. Caricato, X. Li, H. P. Hratchian, A. F. Izmaylov, J. Bloino, G. Zheng, J. L. Sonnenberg, M. Hada, M. Ehara, K. Toyota, R. Fukuda, J. Hasegawa, M. Ishida, T. Nakajima, Y. Honda, O. Kitao, H. Nakai, T. Vreven, J. A. Montgomery, Jr., et al., *Gaussian 09, Revision D.01*, gaussian Inc., Wallingford, CT **2009**.

[45] S. Dapprich, I. Komáromi, K. Byun, K. Morokuma, M. J. Frisch, *J. Mol. Struct.: THEOCHEM* **1999**, *461–462*, 1.

[46] O. Krejčí, P. Hapala, M. Ondráček, P. Jelínek, *Phys. Rev. B* **2017**, *95*, 045407.